Journal of
Applied and Computational Mechanics

Research Paper

Numerical Investigation of an Unsteady and Anisotropic Turbulent Flow Downstream a 90° Bend Pipe with and without Ribs

Rachid Chiremsel[1], Ali Fourar[1], Fawaz Massouh[2], Zakarya Chiremsel[3]

[1] Department of Hydraulics, University of Batna 2, Research Laboratory in Applied Hydraulics, Constantine road N°53.Fesdis, Batna, 05078, Algeria

[2] National Higher School of Arts and Crafts (ParisTech; ENSAM), Laboratory of Fluid Mechanics, France, Email: fawaz.massouh@ensam.eu

[3] Safety Department, University of Batna 2, IHSI-LRPI, Constantine road N°53.Fesdis, Batna, 05078, Algeria, Email: z.chiremsel@univ-batna2.dz

Abstract. In this work, a numerical study of the dynamical behavior of unsteady and anisotropic turbulent flow downstream a 90° bended pipe was presented. For this purpose, comparative computations are carried out employing two flow configurations, bend pipe with ribs and bend pipe without ribs with a curvature radius ratio Rc/D=2.0. In the bend pipe with ribs, the pitch ratios Pt/e=40 and the rib height to pipe diameter e/D is 0.1. This model has been utilized to assess the effect of ribs on flow where the presence of the ribs leads to a complex velocity field with regions of flow separation upstream and downstream of the ribs. The Reynolds-Averaged Navier–Stokes (RANS) approach is employed and the computational model is validated by comparisons with the existing experimental data. The simulations are conducted with the commercials CFD software FLUENT for Dean number varying from 5000 to 40000. The result analysis shows that the higher resistance generated by the ribs produced relatively larger velocity gradient ($\partial U/\partial y$) compared to the case of bend pipe without ribs where a more uniform mean velocity profile is observed. The turbulence intensities are higher in the ribbed bend pipe compared to those in the non-ribbed case and depend faintly on the Dean number. The levels of the Reynolds shear stresses are significantly enhanced by the ribs compared to the case without ribs. This increasing is explained by significantly higher levels of turbulence production over those ribs produced by large values of $\partial U/\partial y$.

Keywords: RANS, Anisotropic, Dean number, Reynolds stresses tensor, RSM.

1. Introduction

Turbulent flows are common physical phenomena, which are very numerous in industrial and natural environments. They are the physical counterpart of the nonlinearity of the Navier-Stokes nonlinear differential equation, which is one of the most important in all physics arising from the fundamental principle of Newton's dynamics associated with the forces applied to a fluid in motion. Despite all the astounding and exceptional observations made by scientists and the existence of credible mathematical models faithfully reflecting turbulence, the latter remains so complex that it is almost impossible for physicists to make a clear statement on the matter.

Turbulent flow in 90° bend pipes is frequently occurring in a variety of industrial applications, such as the pulling pipe of hydraulic turbines, centrifugal pumps, heat exchangers, energy production systems and transport lines. Detailed information about flow through bends pipes can be very valuable for the optimum design of engineering devices by understanding of the qualitative nature of the flow and improving their performance and minimizing the losses. Consequently, a study of unsteady and anisotropic turbulent flows in 90° bend pipes is of great practical importance where an accurate determination of the unsteady characteristics of the turbulent flow is essential for many problems [1]. The flow in such geometries is complex and consists of a primary flow in the axial direction and a secondary flow generated as a result of an imbalance between the centrifugal force and the pressure gradient in the radial direction of curvature. This makes the precise numerical simulation of the flow difficult, in particular for unsteady and anisotropic turbulent flows with high Reynolds number where it is extremely interesting to have knowledge on the expected anisotropy in the flow field [2].

For this reason, the numerical simulation of an unsteady turbulent flow presenting an anisotropy between the turbulent normal stresses and the secondary flows induced by the ribs drawn up across a 90° bend pipe of circular section evoke great scientific interest in the understanding and modeling of the various unsteady phenomena and a certain application interest, notably in the industrial field where the utilizing of the ribs within the pipe causes blockage of flow and produces stronger secondary flows which enhances the radial fluctuations. Therefore, the fluid can be better mixed [3].

Several researchers have studied turbulent flows in bent pipes using theoretical, experimental and numerical methods. Sudo et al. [4] investigated experimentally the turbulent flow in a circular-sectioned 90° bend. The longitudinal, circumferential and radial components of mean and fluctuating velocities and the Reynolds stresses in the pipe cross-section at several longitudinal

stations were obtained. They found that the curvature has a considerable impact on the pressure and velocity distributions. Hüttl and Friedrich [5] observed that the turbulent fluctuations in the curved pipe are drastically reduced compared to flow in a straight configuration and also provided a useful database, albeit at low Reynolds number, for flow modeling for a variety of configurations, including data for few selected terms of the Reynolds stresses. Kawamura et al. [6] measured the velocity field and turbulence intensity field in a 90° elbow with Rc/D=0.55, 1 and 2 at the Re=5×10^4 and 5×10^5 using laser doppler velocimetry (LDV) measurement. They focused on the turbulent intensity and the characteristics of the power spectrum of the turbulent intensity. They presented the important findings that the normalized power spectrum of the turbulent intensity was not affected by the Reynolds number. Though the separation occurred in the case of Rc/D=0.55 and 1, the unsteady flow structure formed by the separation and the secondary flow was not mentioned in detail. Chang and Lee [7] conducted experiments using the two-dimensional particle image velocimetry technique with 21°C water as the fluid. Time-averaged velocity distribution and turbulence intensity of the swirl flow generated by a tangential inlet were obtained for a 90° bent tube for Re=1.0×10^4, 1.5×10^4, 2.0×10^4 and 2.5×10^4. Spedding et al. [8] measured the pressure drop in curved pipes and elbow bends for both laminar and turbulent single-phase flow and developed empirical correlations. The transitional Reynolds number for curved pipes of large bends was also determined using empirical relation. Pruvost et al. [9] investigated the fluid flow in the 90° and 180° bend with a small curvature ratio (Rc/D=0.25) using different turbulence models and wall equations. The results showed that the relation between swirl motion and Dean motion is complicated and swirl motion has an inhibitory effect against Dean motion. Raisee et al. [10] investigated numerically developing turbulent flow through two different 90° curved ducts: a square duct and a rectangular duct. The low-Re models of turbulence are employed. The main objectives of their study are to examine how curvature alters flow development in the curved ducts and to explore the predictive capabilities of a recently modified variant of the cubic non-linear k-ε model, relative to those of the linear low-Re k-ε model, in predicting flow characteristics in curved ducts. According to the conclusions, both models could show a satisfactory prediction of the mean flow field. The nonlinear k-ε model has better performance for turbulence field and pressure and friction coefficients, but it is not accurate for the prediction of flow recovery after the bend exit. Crawford et al. [11] investigated numerically the pressure drop for turbulent flow in 90° elbow bends. Shiraishi et al. [12, 13] measured the pressure fluctuation and observed the flow regime in the pipe with elbow with Rc/D=1 up to the Re=8.0×10^6. Although they concluded that the fluctuating pressure was generated by the movement of the boundary of flow separation and reattachment region, their data of axial velocity profile in the elbow measured by LDV was limited at several positions and not enough to understand clearly the complex and unsteady flow field around the flow separation region. Mojtaba et al. [14] used the Particle Image Velocimetry (PIV) technique that allows reliable measurement of the velocity vectors of the secondary motion in a developing laminar pulsating flow through a curved pipe. Analysis of the vorticity and strain variations during an oscillation period then identifies favorable pulsating conditions that enhance mixing. Ono et al. [15] investigated using water experiments in elbows the mechanism of flow fluctuation induced by the interaction between the flow separation and secondary flow due to the elbow curvature. The elbow curvature ratio was chosen as an experimental parameter in order to change the intensity of the secondary flow induced by the centrifugal force. The time-series of velocity fields in the elbows were measured using a high-speed Particle Image Velocimetry (PIV). Noorani et al. [16] investigated the evolution of the selected characteristics of the turbulent flow in straight to bent pipes over a limited range of Reynolds numbers and curvatures. Min and Zhiguo [17] provided high-resolution velocity maps of the primary and secondary flow upstream and downstream of a 90° bend pipe. The flow field parameters were obtained using numerical methods at the Reynolds number 10000. One of the particular areas of interest is the behavior of the vorticity, turbulent structure, specifically the Dean vortex and swirling flow upstream and downstream of a 90° bend pipe. Niu and Dou [18] used the energy gradient theory to analyze numerical simulation of the flow in a 90° bend with a square cross-section. This study shows that the occurrence of instability is closely related to the evolution of the energy gradient function. Hellström et al. [19] investigated experimentally the secondary flow structures downstream of a 90° bend to try and resolve some of these ambiguities with Reynolds numbers between 2×10^4 and 1.15×10^5. Specifically, they investigated the nature of the swirl switching mode and its relationship to the Dean motions, using snapshot proper orthogonal decomposition (POD). Jongtae et al. [20] performed experimental and numerical studies on turbulent pipe flow after 90° elbows and to characterize the secondary flows induced by the 90° elbows including the dissipation characteristics. Dutta and Nandi [21] studied the pressure drop characteristics of single-phase turbulent flow downstream of the elbow for high Reynolds number (Re=1×10^5 to 10×10^5) and for different curvature ratio (Rc/D=1 to 5) using k-ε RNG turbulence model with standard wall function. Yan et al. [22] predicted by numerical simulation the fluid flows through a curved pipe for Rc/D>0.5. Flow behaviors, such as secondary flow, boundary layer separation and the oscillatory flow, are illustrated and studied. Furthermore, the variation of flow characteristics, such as the turbulence intensity and the secondary flow intensity is estimated for a given flow condition. Röhrig et al. [23] compared RANS and LES simulations to PIV data on cross-sections downstream of the elbow, validating the LES velocity and pressure field calculations. Wang et al. [24] employed Direct Numerical Simulation and studied a turbulent pipe flow with 90° bends. Dutta et al. [25] presented the simulation of the flow pattern in 90° pipe bends with different curvature ratios with different Reynolds numbers. The details of the flow pattern throughout the bend were studied. The variations of velocity profiles with curvature ratio and Reynolds number were studied. The dependency of swirl intensity on a wide range of curvature ratio and Reynolds number are unique features.

This study examines the development of unsteady and anisotropic turbulent flow by considering a circular-sectioned 90° bend pipe with and without ribs. This geometry is of particular interest since it has been the subject of multiple experimental campaigns and numerical studies in recent years which have made it possible to advance in the understanding of the flow topology involved in this hydraulic installation.

The success of a computational result of such flow relies heavily on the choice of the turbulence closure. In the realm of DNS formulation, all degrees of freedom appearing in the flow are considered in all details without any approximation. Nevertheless, one of the major shortcomings of the DNS simulations is their exertion only at low or moderate Reynolds numbers. The LES technique allows to simulate the large turbulent scales and to model the small turbulent scales. The LES predicts both steady and instantaneous phenomena, but requires also very large computer memory and processing time [26]. The RANS modeling approach is intermediate between DNS and LES simulation. Indeed, this approach therefore greatly reduces the required computational effort and resources, and is widely adopted for practical engineering applications [27].

A grid check was carried to ensure that the results are independent of the grid resolution which gives the best compromise between the precision of the results and calculation time. The effect of grid size on the axial velocity was monitored. The validation of the numerical results of the turbulence model is very important to select the suitable turbulence model for the numerical simulation of the analyzed flow. The experiments carried out by Sudo et al. [4] on turbulent flows in 90° bend pipe are used to validate the chosen turbulence model. With this in mind, the RSM turbulence model was selected to evaluate accurately the characteristics of the analyzed flow at the outlet of the bend, but its application to turbulent flows in three-dimensional complex engineering problems requires tremendous computational resources.
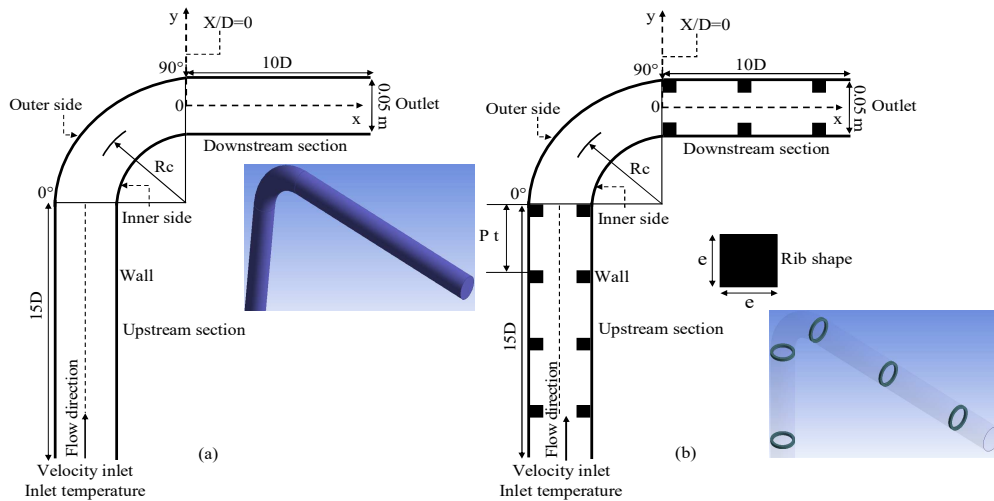
Fig. 1. Schematic representation of bends investigated: (a) 90° bend pipe without ribs, (b) 90° bend pipe with ribs.

Considering the aforementioned, the objectives of this work are, therefore, on the one hand, to study at the exit of the curvature the effect of the 90° bend pipe with and without ribs on hydraulic performance inherent phenomena (velocity distributions, turbulence stresses and turbulence intensities), while carrying out a comparative study between these two geometric models. On the other hand, it is to assess the capacity of the RANS turbulence modeling approach and the RSM turbulence model to accurately reproduce the flow in these systems as part of the numerical simulation of an unsteady and anisotropic turbulent flow by considering a total of four flow conditions. These flow conditions are selected to study the effect of the increase in the Dean number on the behavior of the analyzed flow. The platform used for the current simulations is an Intel® Core™ i5 computer equipped with 6 computing cores and 16 Gb of RAM.

2. Description of the Physical Problem

The problem considered in the current study is the fluid flow characteristics through two circular-sectioned 90° bending pipes having a diameter D of 0.05 m and curvature ratio (Rc/D)=2. For both cases, the lengths of the upstream and downstream sections are 15D and 10D respectively. The first bend pipe is considered without ribs and the second is with square ribs. The number of which is 14 ribs regularly placed along the straight pipe. The pitch ratios Pt/e=40 where Pt is the rib pitch and e is the rib height. The rib height e is 10% of the pipe diameter (e/D=0.1). It is defined that the axial direction downstream the bend is x-coordinate, the direction from the inner core to the outer core of the bend is y-coordinate and the perpendicular direction to x and y is z-coordinate. The geometry of the flow field for both cases is shown in Fig. 1.

3. Governing Conservation Equations of Turbulent Flow

The governing equations, called Navier-Stokes equations, are based on fundamental conservation laws for mass and momentum. For turbulent flow, those equations are three dimensional and time-dependent [28]. In the current study, the Reynolds Averaged Navier-Stokes (RANS) approach is employed for computing turbulent flow. Under consideration of the RANS simulation, three-dimensional governing equations are solved numerically using the finite volume method.

Considering an incompressible and Newtonian fluid, three-dimensional continuity and momentum equations used in this numerical analysis in Cartesian tensor notation can be written respectively as the following:

$$\frac{\partial U_i}{\partial x_i} = 0 \tag{1}$$

$$\frac{\partial U_i}{\partial t} + \frac{\partial}{\partial x_j} U_i U_j = -\frac{1}{\rho}\frac{\partial P}{\partial x_i} + \nu \frac{\partial^2 U_i}{\partial x_j^2} - \frac{\partial}{\partial x_j}\left(\overline{u_i' u_j'}\right) \tag{2}$$

where U_i is the axial mean velocity, P the mean pressure, x_i the coordinate vector, t the time, ρ the density, ν the kinematic viscosity while $\overline{u_i' u_j'}$ denotes the Reynolds stress tensor. The Reynolds averaging equations are preceded by a decomposition of the instantaneous values of velocity and pressure into a mean and a turbulent fluctuating quantity, i.e.

$$u_i = U_i + u_i' \tag{3}$$

where u_i is the instantaneous velocity and u_i' denotes the fluctuating velocity.

$$p_i = P_i + p_i' \tag{4}$$

where p_i is the instantaneous pressure, P_i the mean pressure and p_i' the fluctuating pressure.

Thus the averaging process introduced a new unknown tensor term $\overline{u_i' u_j'}$ that appears in the RANS equations (eq. (2)). It comes from the non-linearity of the convection term of the Navier-Stokes equations. Consequently, the set of equations is no longer closed. This is called the closure problem of averaging approaches. It will therefore naturally be necessary to find new equations to solve the system allowing numerical solutions to be obtained. In three dimensions, this tensor is noted as the following:

$$\overline{u_i^{'} u_j^{'}} = \begin{bmatrix} \overline{u^{'} u^{'}} & \overline{u^{'} v^{'}} & \overline{u^{'} w^{'}} \\ \overline{u^{'} v^{'}} & \overline{v^{'} v^{'}} & \overline{v^{'} w^{'}} \\ \overline{u^{'} w^{'}} & \overline{v^{'} w^{'}} & \overline{w^{'} w^{'}} \end{bmatrix} \tag{5}$$

3.1 Turbulence Modelling Equations

In order to close the RANS equations, a model of turbulence must be provided. The transport equations include a number of unknowns. The aim of turbulence modeling is to treat these unknowns in terms of the physically known properties. It is now accepted that, without modification, conventional turbulent viscosity models are incapable to faithfully reproduce the behavior of secondary flows, whereas the Reynolds stress model has proved capable of predicting such flows. This means that the isotropic turbulent viscosity models (conventional turbulent viscosity models) are absolutely dissipative. Thus, the two-way transfer of turbulent kinetic energy between mean motion and turbulent motion cannot be maintained [29].

Another weakness of the turbulent viscosity models is the representation of the three normal turbulent stresses by their sum, which amounts to admitting a similar evolution of these three components, even if the turbulent anisotropy of the flow can be contained in the modeling. Therefore, in flows where the three normal stresses vary very differently, the conventional turbulent viscosity models, even with two equations, are not always very satisfactory [30]. Consequently, the application of this type of models leads to mal prediction of the normal Reynolds stresses.

A clear advantage of RSM model compared to the turbulent viscosity models is that the production term does not require approximations. It is the production term that is primarily responsible for the anisotropy. Hence, it is expected that this higher level of modeling, representing more elaborate physics, would be beneficial in terms of accurate flow predictions. One of the main characteristics of second-order closings lies in the possibility of representing the different mechanisms that govern the evolution of double correlations [31].

In this paper, the Reynolds stress model (RSM) is proposed, the latter proved to be able to predict the anisotropy of turbulent flows [32]. RSM is theoretically more adapted when turbulence is found to be anisotropic, as in bend flows [33]. Solving three-dimensional equations by means of this model is extremely complicated [26], where the differential transport equations are solved for each Reynolds stress component which requires more effort and time to simulate the flow. These equations include some terms that are exact and some that must be modeled [34]. The modeled terms require a variety of ad hoc wall damping functions and the numerical values of the coefficients are chosen based on empiricism [26]. However, the complexity of numerical models and numbers of degrees of freedom increase to a demanding task regarding disk space and CPU time [35]. The exact transport equations for the transport of the Reynolds stresses $\overline{u_i^{'} u_j^{'}}$ may be written as follows [36]:

$$\frac{\partial \overline{u_i^{'} u_j^{'}}}{\partial t} + U_k \frac{\partial \overline{u_i^{'} u_j^{'}}}{\partial x_k} = \nu \frac{\partial^2 \overline{u_i^{'} u_j^{'}}}{\partial x_k \partial x_k} - \frac{\partial \overline{u_i^{'} u_j^{'} u_k^{'}}}{\partial x_k} - \frac{1}{\rho} \overline{u_i^{'} \frac{\partial p^{'}}{\partial x_j}} -$$
$$\frac{1}{\rho} \overline{u_j^{'} \frac{\partial p^{'}}{\partial x_i}} - \overline{u_i^{'} u_k^{'}} \frac{\partial U_j}{\partial x_k} - \overline{u_j^{'} u_k^{'}} \frac{\partial U_i}{\partial x_k} - 2\nu \overline{\frac{\partial u_i^{'}}{\partial x_k} \frac{\partial u_j^{'}}{\partial x_k}} \tag{6}$$

where $\overline{u_i^{'} u_j^{'} u_k^{'}}$ is the triple correlations of fluctuating velocities. Equation (6) can be written in the following form [37]:

$$\frac{D \overline{u_i^{'} u_j^{'}}}{Dt} = P_{ij} - \varepsilon_{ij} + \Phi_{ij} + D_{ij}^T + D_{ij}^{\nu} \tag{7}$$

where the turbulent production, convection, viscous dissipation, velocity-fluctuating pressure correlation, turbulent diffusive transport and molecular diffusion are defined, respectively, as:

$$P_{ij} = -\overline{u_i^{'} u_k^{'}} \frac{\partial U_j}{\partial x_k} - \overline{u_j^{'} u_k^{'}} \frac{\partial U_i}{\partial x_k} \tag{8}$$

$$C_{ij} = U_k \frac{\partial \overline{u_i^{'} u_j^{'}}}{\partial x_k} \tag{9}$$

$$\varepsilon_{ij} = 2\nu \overline{\frac{\partial u_i^{'}}{\partial x_k} \frac{\partial u_j^{'}}{\partial x_k}} \tag{10}$$

$$\Phi_{ij} = -\frac{1}{\rho} \overline{u_i^{'} \frac{\partial p^{'}}{\partial x_j}} - \frac{1}{\rho} \overline{u_j^{'} \frac{\partial p^{'}}{\partial x_i}} \tag{11}$$

$$D_{ij}^T = -\frac{\partial \overline{u_i^{'} u_j^{'} u_k^{'}}}{\partial x_k} \tag{12}$$

$$D_{ij}^{\nu} = \nu \frac{\partial^2 \overline{u_i^{'} u_j^{'}}}{\partial x_k \partial x_k} \tag{13}$$

The terms C_{ij}, D_{ij}^{υ} and P_{ij} can be preserved in their exact form, no modeling is necessary. However the terms D_{ij}^T, ϕ_{ij} and ε_{ij} require modeling that provides mathematical relationships to close the system. For the ε-based RSM, D_{ij}^T can be modeled as follows [38]:

$$D_{ij}^T = \frac{\partial}{\partial x_k}\left(\frac{\mu_t}{\sigma_k}\frac{\partial \overline{u_i' u_j'}}{\partial x_k}\right) \tag{14}$$

where the σ_k is an empirical constant and μ_t is the turbulent viscosity which is computed by the equation:

$$\mu_t = \rho C_\mu \frac{k^2}{\varepsilon} \tag{15}$$

where k is the turbulent kinetic energy, ε is the turbulence dissipation rate and C_μ is an empirical constant.

By default in ANSYS Fluent, the pressure-strain term, Φ_{ij} is modeled according to the proposals by Gibson and Launder [39], Fu et al. [40] and Launder [32]. The classical approach to modeling Φ_{ij} uses the following decomposition:

$$\Phi_{ij} = \Phi_{ij,1} + \Phi_{ij,2} + \Phi_{ij,w} \tag{16}$$

where $\Phi_{ij,1}$ is the slow pressure-strain term, also known as the return to isotropy term.
This term is modeled as:

$$\Phi_{ij,1} = -C_1 \rho \frac{\varepsilon}{k}\left(\overline{u_i' u_j'} - \frac{2}{3}\delta_{ij}k\right) \tag{17}$$

The term $\Phi_{ij,2}$ is called the rapid pressure-strain, it is modeled as:

$$\Phi_{ij,2} = -C_2\left(\left(P_{ij} - C_{ij}\right) - \frac{1}{3}\delta_{ij}\left(P_{kk} - C_{kk}\right)\right) \tag{18}$$

where δ_{ij} is the Kronecker symbol, C_1 and C_2 are the empirical constants.

The term $\Phi_{ij,w}$ is the wall-reflection, it is responsible for the redistribution of normal stresses near the wall. It tends to damp the normal stress perpendicular to the wall while enhancing the stresses parallel to the wall [41]. This term is modeled as:

$$\Phi_{ij,w} = C_1'\frac{\varepsilon}{k}\left(\overline{u_k' u_m'}n_k n_m \delta_{ij} - \frac{3}{2}\overline{u_i' u_k'}n_j n_k - \frac{3}{2}\overline{u_j' u_k'}n_i n_k\right)\frac{C_\mu^{3/4}k^{3/2}}{\varepsilon d \kappa} +$$
$$C_2'\left(\Phi_{km,2}n_k n_m \delta_{ij} - \frac{3}{2}\Phi_{ik,2}n_j n_k - \frac{3}{2}\Phi_{jk,2}n_i n_k\right)\frac{C_\mu^{3/4}k^{3/2}}{\varepsilon d \kappa} \tag{19}$$

where n_k is the unit vector normal to the wall, d is the normal distance to the wall, κ the von Kármán constant while C_1' and C_2' denote an empirical constants.

For Reynolds stress models based on the ε-equation, the dissipation tensor ε_{ij} is modeled as:

$$\varepsilon_{ij} = \frac{2}{3}\delta_{ij}\left(\rho\varepsilon + Y_M\right) \tag{20}$$

where Y_M is an additional dilatation dissipation term according to the model of Sarkar and Balakrishnan [42].

$$Y_M = 2\rho\varepsilon M_t^2 \tag{21}$$

where M_t is the turbulent Mach number. It is defined as:

$$M_t = \sqrt{\frac{k}{a^2}} \tag{22}$$

where a is the speed of sound.

The scalar dissipation rate ε is computed with a model transport equation similar to that used in the standard k-ε model, it is found by solving its transport equation [41]:

$$\frac{\partial}{\partial t}(\rho\varepsilon) + \frac{\partial}{\partial x_i}(\rho\varepsilon u_i) = \frac{\partial}{\partial x_j}\left[\left(\mu + \frac{\mu_t}{\sigma_\varepsilon}\right)\frac{\partial \varepsilon}{\partial x_j}\right] + C_{\varepsilon 1}\frac{P_{ii}}{2}\frac{\varepsilon}{k} - C_{\varepsilon 2}\rho\frac{\varepsilon^2}{k} \tag{23}$$

where μ is the dynamic viscosity which may significantly impact the dynamics. It is a function of the temperature of the fluid where its decreases by the increase of the liquid temperature conduct to the reduction of the pressure drop [43]. σ_ε, $C_{\varepsilon 1}$ and $C_{\varepsilon 2}$ denote an empirical constants.

The constant values for the Reynolds stress model are given in Table 1.

Table 1. Empirical constants for the RSM model.

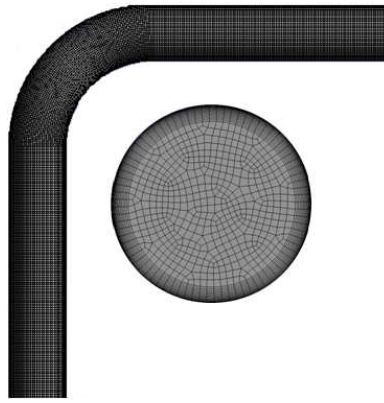| C_μ	σ_k	C_1	C_2	C_1'	C_2'	κ	σ_ε	$C_{\varepsilon 1}$	$C_{\varepsilon 2}$
0.09	0.82	1.8	0.6	0.5	0.3	0.4187	1.0	1.44	1.92

Fig. 2. Computational grid of the bends flow.

4. Mesh Generation and Grid Independence Study

In this study, 3D structured hexahedral meshes with inflation near the walls are used for both geometries considered as shown in Fig. 2. This type of mesh presents a capability in providing a high-quality solution with fewer numbers of cells, higher accuracy and reduce CFD computational effort [44]. However, a discretization mesh of the flow is one of the most difficult phases because the quality of the mesh depends on the accuracy of the numerical simulation. Furthermore, one cannot ignore the constraints of the computing capacity, namely, those that limit the number of mesh nodes and the size of the mesh elements [45]. Using the sizing functions, a high adaptive mesh density was maintained in the bend and the regions close to the wall and ribs where the mesh is stretched from the solid wall toward the centerline to gain a higher resolution near the wall, where better resolution is needed [46]. The value of non–dimensional distance from the wall (y+) is controlled using a wall treatment function (y+<5 for a near wall cell used for the present study). The size and the number of layers are selected to provide the y+ wall distance for the predicted high Reynolds y+ treatment [47]. The wall treatment used for all of the computations reported is the standard wall function approach. The grid generation is a key issue in flow simulation that governs the stability, the accuracy of the predictions and the time of CFD numerical computation. A very fine grid is computationally more expensive and is necessary to ensure reasonable resolution of the mesh [48]. The appropriate quality and quantity of grids are very important. For the mesh independence study, five levels of refinement are generated by using ANSYS ICEM to optimize the mesh convergence by studying the effects of grid numbers on the stability of numerical results and ensure that the solution is independent of the mesh. They are reported in Table 2.

The convergence criterion used for these calculations is 10^{-6} for all flow equations.

In Figure 3, the mean axial velocity profile at X/D=0 is used in a grid independence test where X is defined as the position on the longitudinal axis, R is the radius of the pipe and r denotes the radial distance, the Dean number is De=3×10^4. Based on the results, it appears that the distribution of the mean axial velocity U_x normalized by the inlet velocity u_{in} (U_x/u_{in}) obtained for the mesh-5 does match with the profile obtained for the mesh-4. It can be clearly observed that the relative deviation of axial velocity between mesh-4 and mesh-5 is only 0.078% relative error, which is acceptable in most engineering analyses and designs. Hence there is no need to refine the mesh any further and the mesh-4 is accepted for computations of the present study. The Table 3 summarizes the statistics of the mesh-4.

The mesh quality is verified through skewness property. Referring to Table 4, the mesh quality is excellent, where the metric skewness is equal to 0.0698. The following table lists the range of skewness values and the corresponding cell quality.

Table 2. Error analysis of various grid sizes.

Mesh	Number of nodes	Number of elements	Skewness	Error(%)
Mesh1	602745	140070	0.1448	6.38
Mesh2	1605075	390264	0.0905	3.84
Mesh3	4019697	981834	0.0815	1.79
Mesh4	6234372	1534929	0.0698	0.078
Mesh5	12241833	3018520	0.0646	-

Table 3. Details of mesh.

Inflation Option	Smooth Transition
Maximum Layer	20
Growth Rate	1.2
Nodes	6234372
Elements	1534929
Mesh Metric	Skewness
Min	0.0048
Max	0.4298
Average	0.0698
Standard Deviation	0.0652

Table 4. Classification of the mesh quality metrics based on skewness [49].

0-0.25	0.25-0.50	0.50-0.75	0.75-0.9	0.9-1	1
Excellent	Good	Fair	Poor	Bad(sliver)	Degenerate

Table 5. Measurement errors (%).

	RSM		Standard k-ε	
X/D	Maximum error (%)	Average error (%)	Maximum error (%)	Average error (%)
0	5.34	1.27	7.69	3.08
0.5	5.75	1.22	6.59	1.82
1	5.95	1.02	5.88	1.90
2	5.54	1.15	5.76	1.67
5	13.66	13.49	13.61	13.57

4.1 Validation of Model

After establishing grid independence, the selection of an appropriate turbulence model for the numerical simulation of an unsteady and anisotropic turbulent flow in a bend pipe is very important. For it, the RSM and standard k-ε models have been employed. Results and simulation setup are firstly validated against the available experimental data with air as the working fluid [4] where the measurements of velocities were performed at a Dean number of 3×10^4. It can be seen that a reasonably good agreement has been obtained between the predictions by all two turbulence models and the experimental data as presented in Fig. 4. Nevertheless, the prediction by the RSM model is closer to the experimental data, especially the peak value is most accurately captured while it is underestimated by the standard k-ε model.

The four evolutions are perfectly superimposed and the observed difference between the different results is barely remarkable where for X/D=0, X/D=0.5, X/D=1 and X/D=2, the maximum errors of mean axial velocity differences range between 5% and 6% where a similar behavior is observed with the published results however at X/D=5 the errors is around 14%. This translates that in the case of experimental data of Sudo et al. [4], the mean axial velocity profile is significantly altered by the flow's weakening. Although the experimental data do not show a fully-developed state being reached downstream the bend, it appears to be approaching such a condition by the point X/D=5. While, in the present simulation neither model correctly predicts the mean axial velocity profile in the point X/D=5, the flow is still accelerated and a further longitudinal distance is required for the flow to be fully developed turbulent.

The estimates of errors are summarized in the Table 5. In view of the above, the trends for the mean axial velocity profiles are well captured properly and accurately by the RSM model which appears superior in predicting the axial velocity peak; this is due that the RSM model was formulated by involving the strong anisotropic turbulent flows. Overall the RSM performs best for this it has been used for the rest of this study.
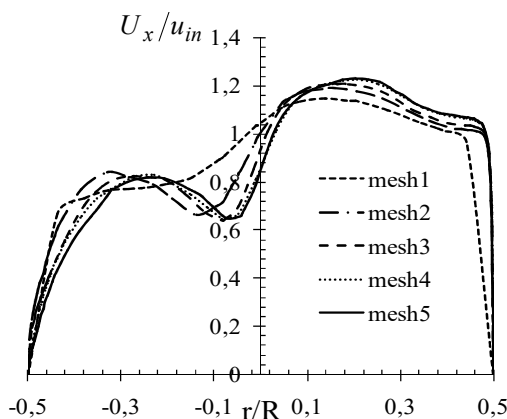

Fig. 3. Normalized mean axial velocity distribution for different structured meshes.
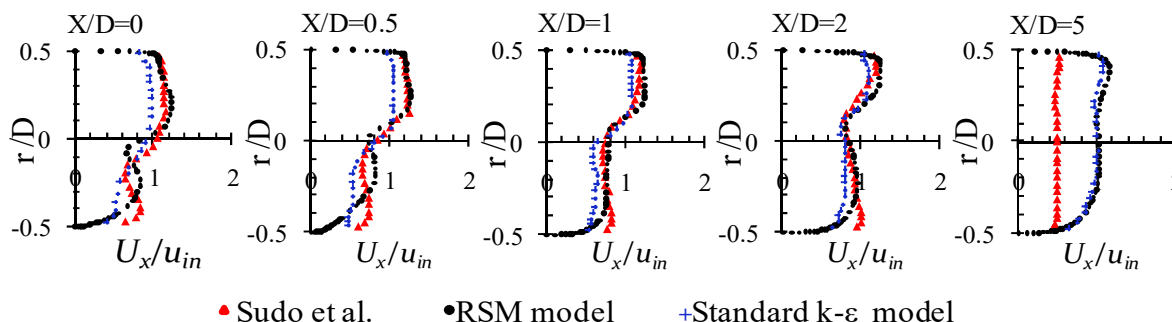

Fig. 4. Comparisons of the non-dimensional mean axial velocity profiles with experimental data of Sudo et al. [4], along the symmetry line, at different sections downstream of the bend.

Table 6. List of flow conditions investigated in the current study.

Flow conditions	De	u_{in} (m/s)	k_{in} (m²/s²)	ε_{in} (m²/s³)	I (%)
Run 1	5000	0.200	0.0001500	1.102E-5	5
Run 2	10000	0.402	0.0005129	6.969E-5	4.60
Run 3	20000	0.804	0.0017514	4.399E-4	4.25
Run 4	40000	1.608	0.0058990	2.718E-3	3.90

Table 7. Thermophysical properties of the fluid at T=293k [54].

ρ (kg/m³)	cp (J.kg⁻¹.K⁻¹)	K (W m⁻¹ k⁻¹)	µ (kg/(m s))
998.21	4182	0.6024	0.001003

Table 8. List of flow run calculations investigated in the current simulations.

Flow conditions	Bend pipe without ribs		Bend pipe with ribs	
	Time step size	Number of time steps	Time step size	Number of time steps
Run 1	18.970E-4	3708	20.810E-4	3381
Run 2	09.438E-4	3708	10.353E-4	3381
Run 3	04.719E-4	3708	05.177E-4	3381
Run 4	02.359E-4	3708	02.588E-4	3381

5. Boundary Conditions and Numerical Details

The resolution of the nonlinear governing equations presented above, is done by the use of the defined boundary conditions which are described in Fig. 1. A total of four flow conditions, as shown in Table 6, are studied in this paper. Inlet boundary conditions applied in entry are defined in terms of velocity, temperature, turbulent kinetic energy and specific dissipation rate. The velocity at the inlet was calculated based on the Reynolds number referred to the pipe diameter and entrance flow conditions. The Reynolds number is an important dimensionless quantity in fluid mechanics which is used to predict transition from laminar, sheet-like flow in parallel layers to turbulent flow which is characterized with unsteady vortices [50]. When the Reynolds number increases, the working fluid quickly leaves the pipe [51] which affect the velocity profile and as a result the temperature profile too where it is observed that enhancement of heat transfer is particularly notable at low Reynolds numbers [52]. The fluid inlet temperature was fixed at 293k. The values of the turbulent kinetic energy and its specific dissipation rate are calculated from the inlet turbulence intensity and pipe diameter using the following equations respectively [21]:

$$k_{in} = 1.5 \left(Iu_{in} \right)^2 \tag{24}$$

$$\varepsilon_{in} = \left(C_\mu k^{1.5} \right) / 0.3D \tag{25}$$

where the turbulence intensity has been calculated using the following formula [53]:

$$I = 0.16 \, \mathrm{Re}^{-0.125} \tag{26}$$

$$\mathrm{Re} = \frac{u_{in}D}{\nu} \tag{27}$$

At the pipe wall no slip boundary conditions for the velocity has been applied and the wall was treated as stationary. The outlet was given as outflow and the working fluid (water) was supposed to be incompressible with constant properties summarized in Table 7 where cp denotes the specific heat and k is the thermal conductivity. The flow was assumed to be three-dimensional turbulent, unsteady and anisotropic.

In the analysis of flows through bend pipes, the Dean number is used frequently. It is defined according to the following equation:

$$\mathrm{De} = \mathrm{Re} \sqrt{\frac{D}{2Rc}} \tag{28}$$

where Rc is the radius of curvature and Re is the Reynolds number.

The second-order upwind scheme was implemented for the solution of momentum terms. The SIMPLE algorithm is used for pressure-velocity coupling. The time step size and the number of time steps used in current simulations considering established flow conditions are summarized in Table 8. The run time of each simulated case is approximately 5 days. The Solutions of these flows were obtained using the software ANSYS FLUENT Release 19.0 with a Dean number ranging from 5000 to 40000. The setup of FLUENT was mentioned graphically in Fig. 5. Analysis results at different locations downstream of the bend were used in this study.

6. Results and Discussion

The main objective of the current study is, on the one hand the comparison of the hydrodynamic behavior of unsteady and anisotropic single-phase turbulent flows into 90° bend pipe without and with ribs through numerical simulation along the different positions downstream of the bend and on the other hand, it is to investigate how the ribs affect the turbulence characteristics of the analyzed flow, such as turbulence intensities and Reynolds shear stresses. The results are reported in terms of the normalized axial velocity, turbulence intensities and Reynolds shear stresses as a function of Dean number ranging from 5×10^3 to 40×10^3.
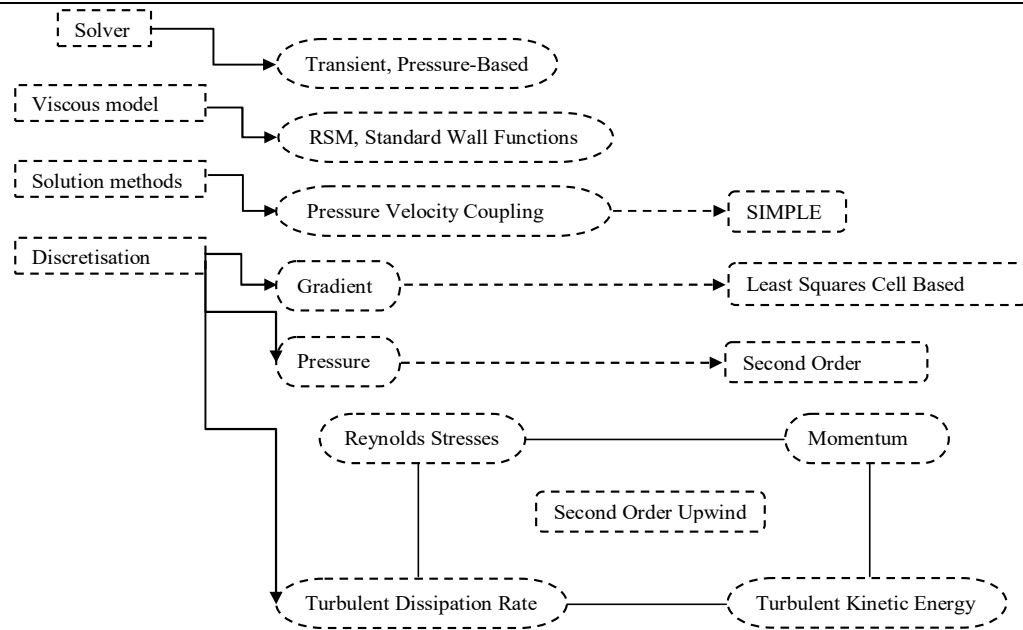
Fig. 5. Set up of FLUENT.

6.1 Mean Velocities

The distributions of mean axial velocity normalized by the inlet velocity u_{in} and its evolution with the increasing of downstream location and the Dean number are presented in Fig. 6. The negative r values represent the inner core of the bend and the positive values represent the outer core. The data displayed are taken in the symmetry plane of the configuration according to the coordinate r which extends perpendicular to the centerline.

An examination of this figure shows that for the two geometric models considered, the distribution of the mean axial velocity does not present any great difference between the different Dean numbers used, which means that there is a similarity in the structure of the analyzed flow after the elbow with the radius of curvature adopted if the Dean number is between 5000 and 40000. We deduce that for the bend pipe with a small curvature ratio (Rc/D≤2) the Dean number is found as a weak function.

For the case of bend without ribs Fig. 6, the study shows a significant shift of the peak velocity towards the outer wall just at the exit of the bend up to a distance X=2.5D. The velocity profile has an inflection point corresponding to a change in concavity causing a rate of increase in acceleration towards the outer wall of the pipe. This acceleration is due to the pressure gradients that develop at the entrance to the elbow due to the centrifugal force. The main characteristic of this flow in this area is the appearance of camel back shapes in the distribution of velocity. These forms are the result of the loss of momentum.

By moving away from the bend and from X=5D, we see that the flow tends to regain its fully developed form, the velocity profile is approximately symmetrical (flattened form) and similar behavior has been observed.

According to the simulation results, an increase of the mean axial velocity in the centerline of the pipe is observed in the ribbed bend pipe where it is found that the velocity profile has a clearly peak. This increase is caused by blockage of cross-section of the fluid flow in pipe with the presence of the ribs that causes flow acceleration, disturbance in the full pipe flow and affects the main stream velocity by creating more turbulence. This suggests also that, the redistribution of the kinetic energy among its components is altered by ribs. Relative to the non-ribbed case, the flow is not disturbed.

Finally, there is a clear trace and impact of the ribs on turbulence. This would indicate that the acceleration of the velocity is higher for the ribbed bends pipe. The fluid moves more quickly at the central region of the pipe as it is viewed in Fig. 6 which shows that the maximum velocity value is approximately 47% higher than the corresponding upstream value but it is 9% higher in the case of the bend pipe without ribs.

It is found that the fluid is somewhat displaced towards the exterior surface of the wall. Consequently, the flow tends to regain its fully developed form in the inner heart downstream the bend by slowing the effects thanks to the ribs placed upstream and downstream of the bend where the flattened form in the central part of the pipe is observed at X=D. The recovery of the profile seems to be caused by turbulent transport, which should be more important in the presence of ribs.

We observed a secondary flow structure composed of two counter-rotating cells located downstream of the second rib at X=8.5D. These vortices appear to be induced near the inner and outer walls of the cross-section for a short time.

Figure 7 shows the velocity contours for different cross-sections downstream of the bend considering a Dean number De=40000. It appears that moving away from the downstream, the fluid in the central region of the pipe moves towards the outer wall due to the centrifugal force (see Fig. 7(a)). The position of the flow shows that the greatest axial velocity changes are seen by going towards the outer wall however in the case of the bend pipe with ribs, near the top and bottom walls of the pipe, the fluid moves more slowly than that near the central plane due to the presence of ribs where the flow is more accelerated pushes the fluid in the boundary layer towards the walls (see Fig. 7(b)), this, therefore, requires a smaller pressure gradient to balance the centrifugal force.

6.2 Turbulence Intensities

A turbulence analysis should include the turbulence intensities, which is the primary metric to characterize the turbulence. The effects of turbulence downstream of the bend are presented as turbulence intensities of the flow that is a measure of the relative importance between the velocity fluctuation and the mean flow. For both cases considered without and with ribs, the profiles of the turbulence intensities are plotted at different positions downstream the bend while considering a Dean number in the range 5000 to 40000. The profiles of streamwise turbulent intensity $\sqrt{u'u'}/u_{in}$ and tangential turbulent intensities $\sqrt{v'v'}/u_{in}$, $\sqrt{w'w'}/u_{in}$ normalized by the inlet velocity u_{in} are shown in Fig. 8 to 10 respectively.
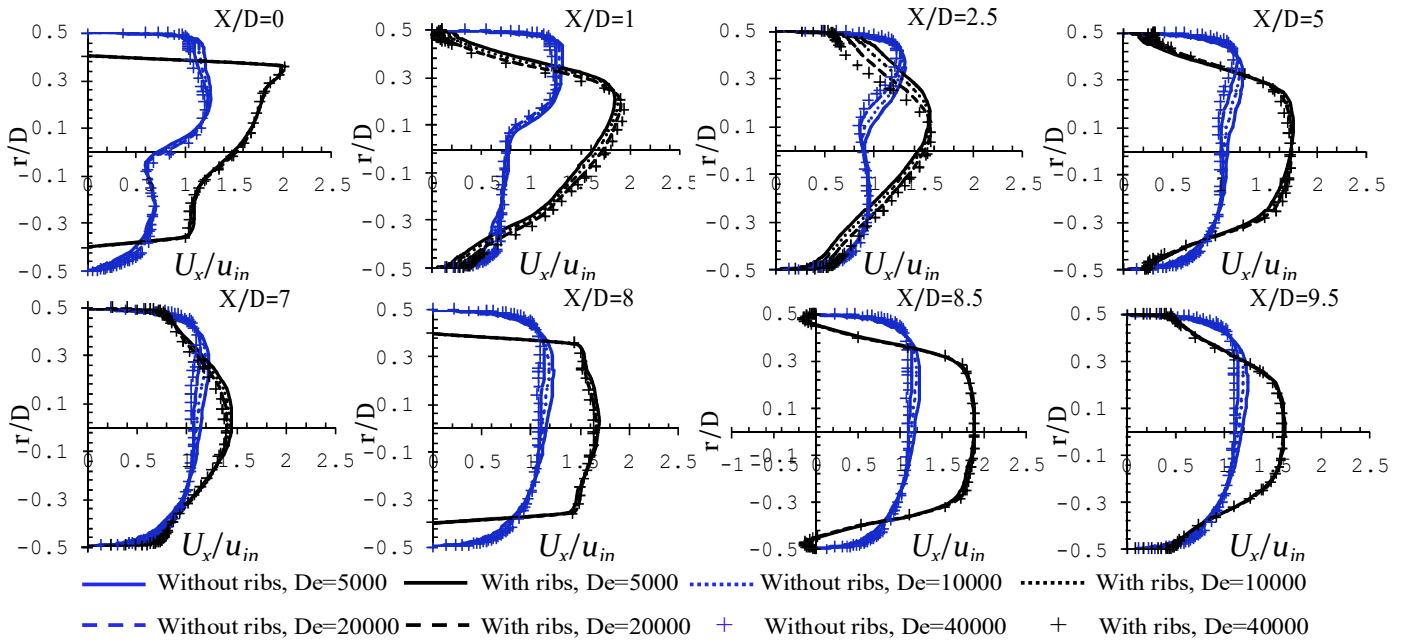
Fig. 6. Comparison of normalized mean axial velocity profiles at different locations downstream the bends with and without ribs obtained with RSM model, De=5000, 10000, 20000 and 40000.
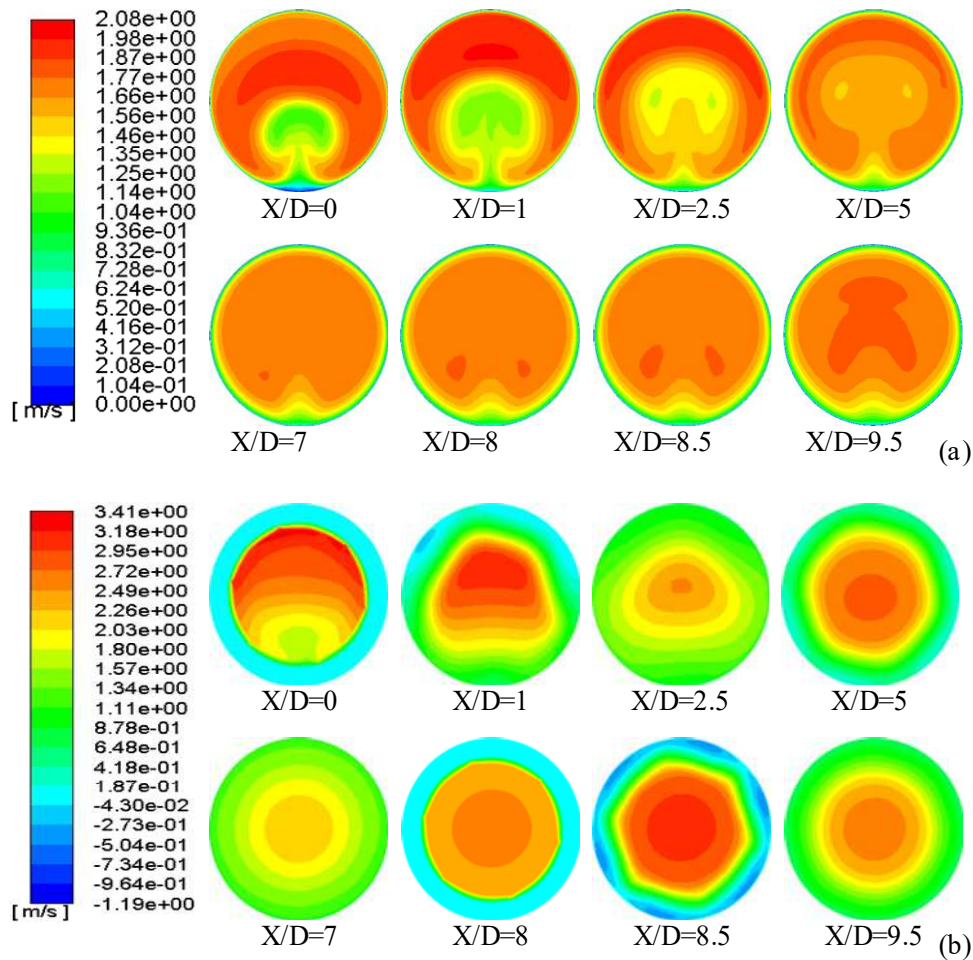

Fig. 7. Streamwise velocity contours for De=40000 at different sections downstream of the bend. (a) bend pipe without ribs, (b) bend pipe with ribs.
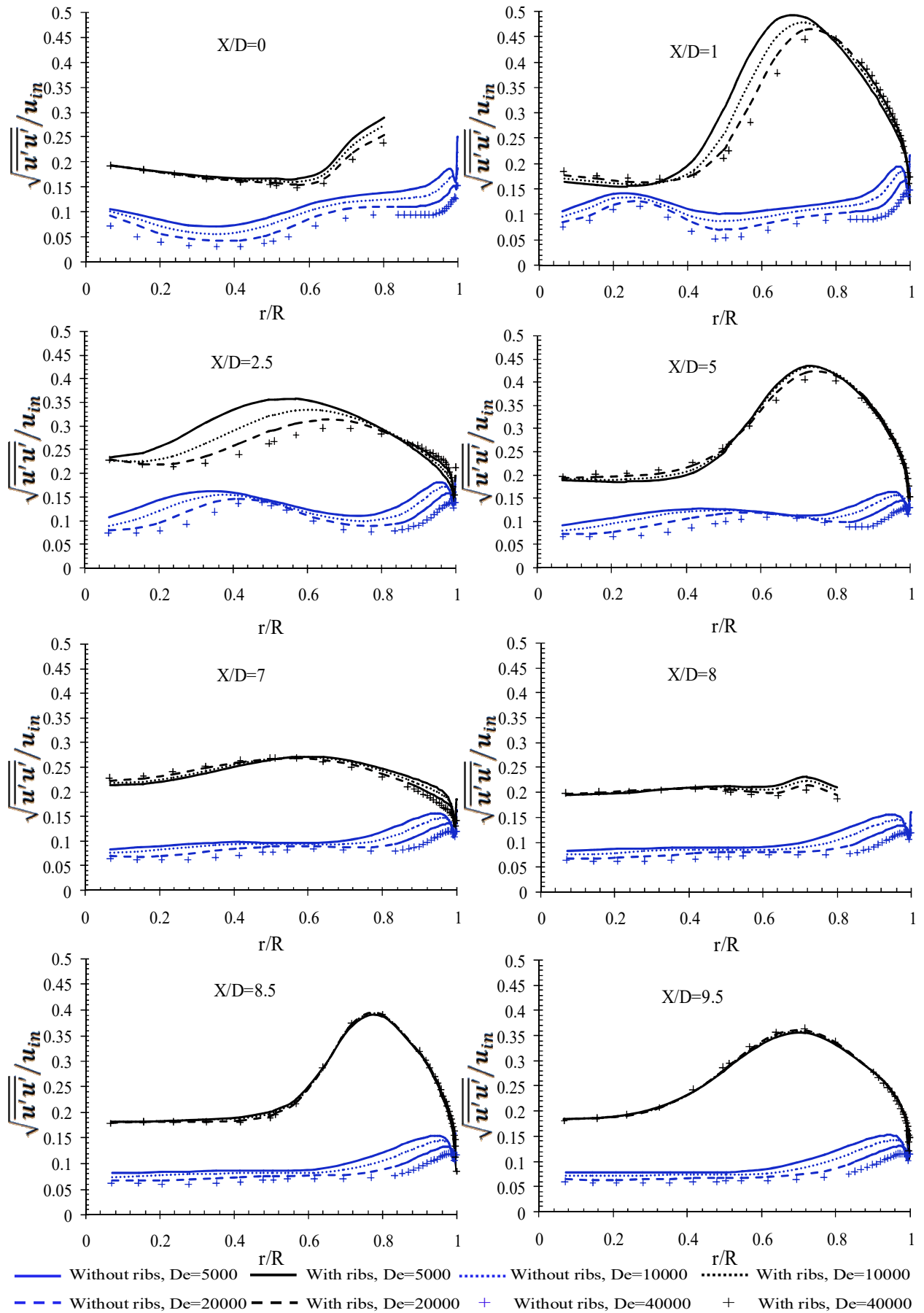
Fig. 8. Comparison of the normalized longitudinal turbulent intensity $\sqrt{\overline{u'u'}}\,/\,u_{in}$ distributions for ribbed and non-ribbed bend pipe at selected locations downstream the bend, De=5000, 10000, 20000 and 40000.
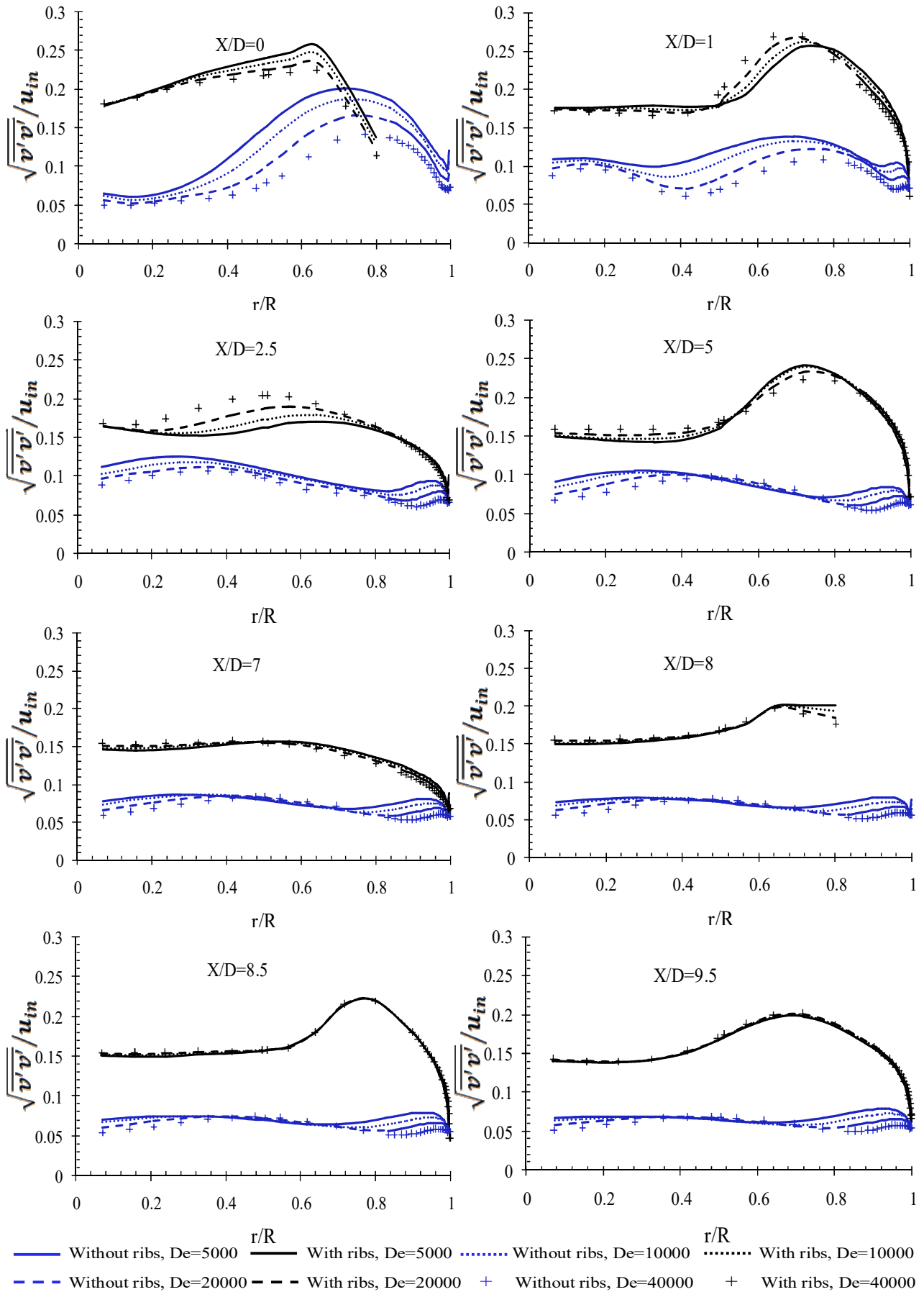
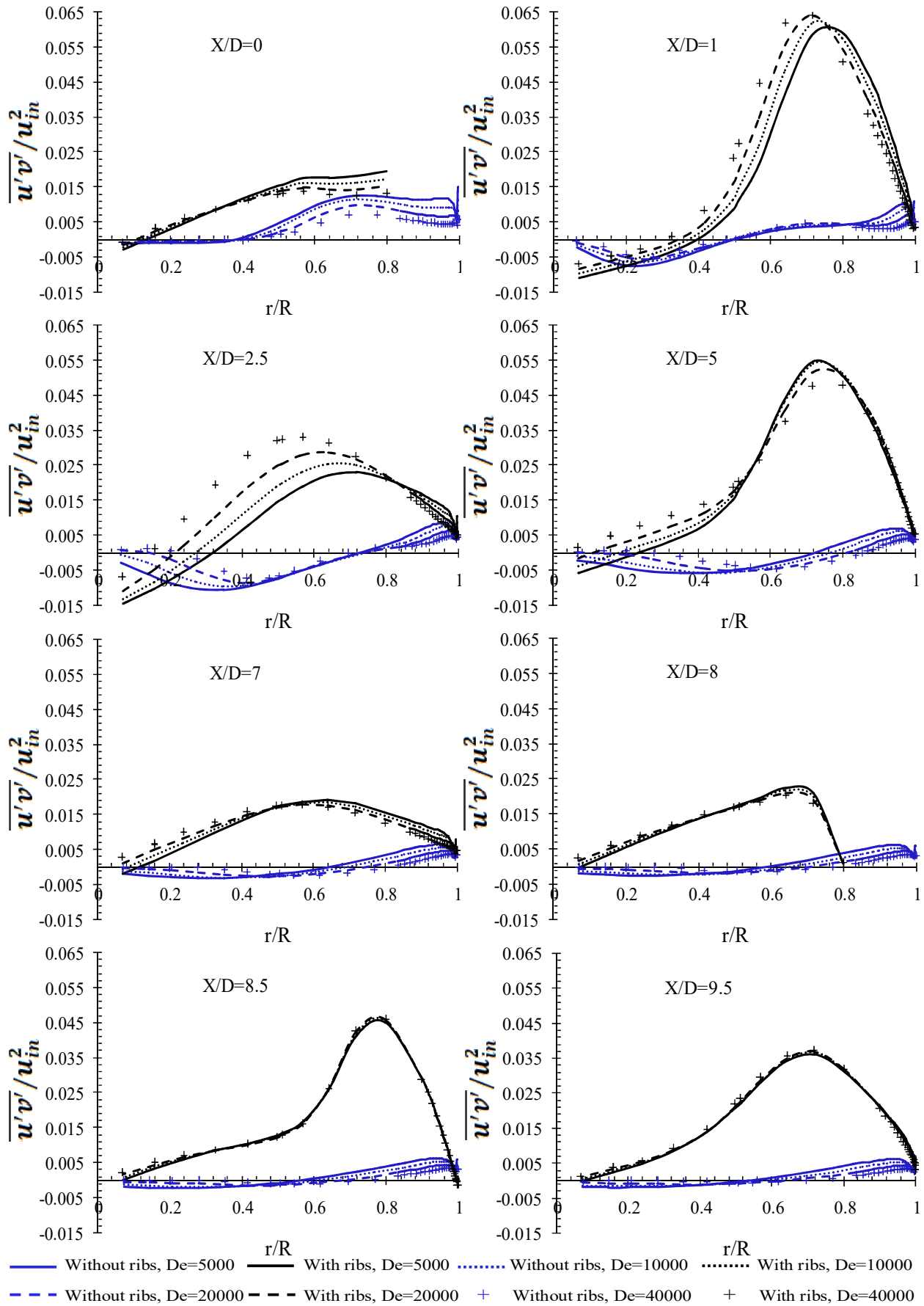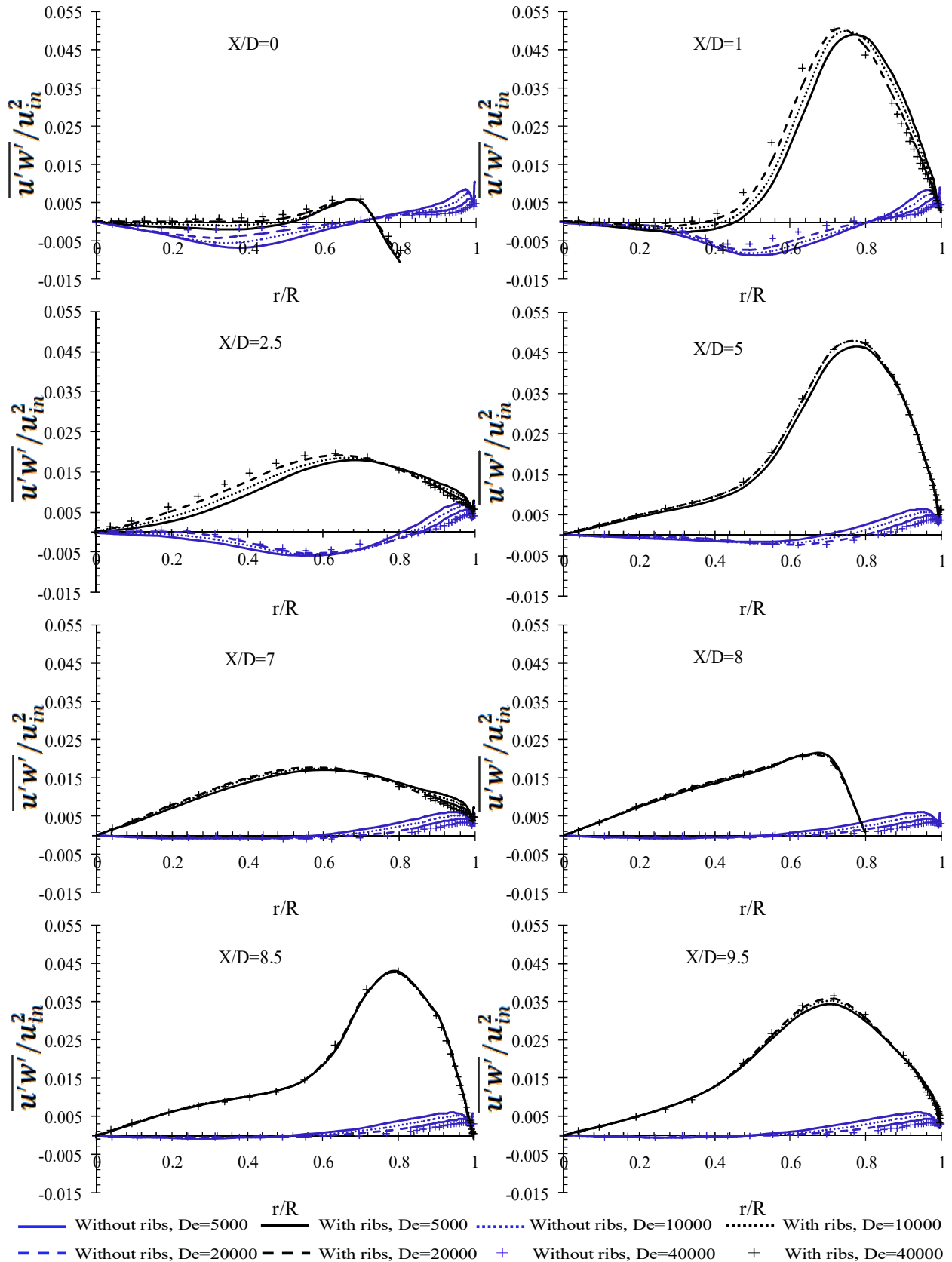**Fig. 9.** Comparison of the normalized transverse turbulent intensity $\sqrt{\overline{v'v'}} / u_{in}$ distributions for ribbed and non-ribbed bend pipe at selected locations downstream the bend, De=5000, 10000, 20000 and 40000.
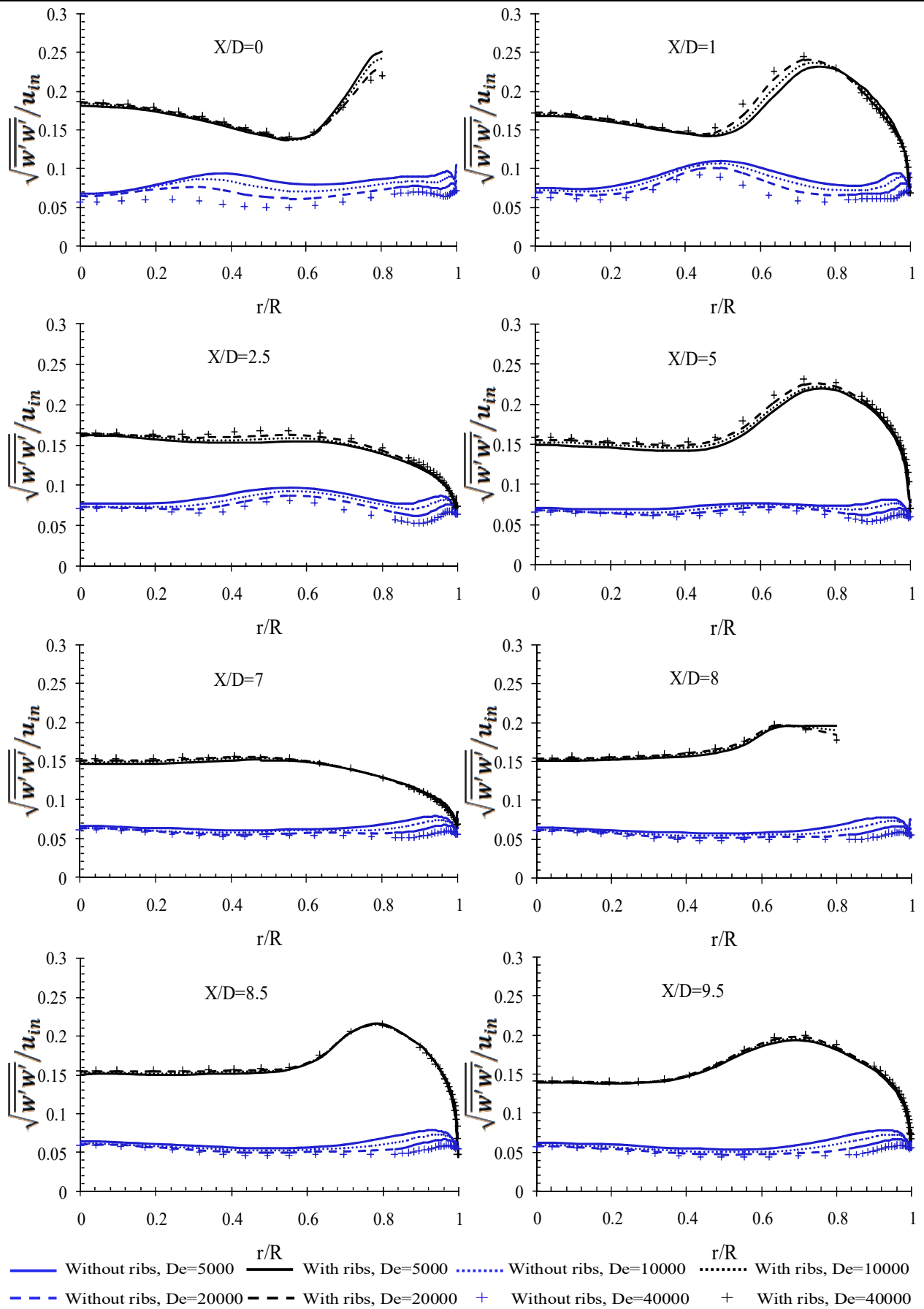
Fig. 10. Comparison of the normalized transverse turbulent intensity $\sqrt{\overline{w'w'}}\,/\,u_{in}$ distributions for ribbed and non-ribbed bend pipe at selected locations downstream the bend, De=5000, 10000, 20000 and 40000.

Fig. 11. Comparison of the normalized Reynolds shear stress $\overline{u'v'}\,/\,u_{in}^2$ distributions between the ribbed and non-ribbed bend pipe at selected locations downstream the bend, De=5000, 10000, 20000 and 40000.

Fig. 12. Comparison of the normalized Reynolds shear stress $\overline{u'w'}/u_{in}^2$ distributions between the ribbed and non-ribbed bend pipe at selected locations downstream the bend, De=5000, 10000, 20000 and 40000.

By examining Fig. 8 to 10 and considering the case of the bend pipe without ribs, the turbulence intensities are in a range from 7% to 15% of the inlet velocity u_{in} however in the ribbed bend pipe case, the streamwise turbulent intensity varies between 15% and 45% and the tangential turbulent intensities are in a range from 15% to 25% of the inlet velocity u_{in}.

Considering the case of the bend pipe without ribs, it is observed that in the center line and going towards the walls, the

streamwise and tangential turbulence intensities remained almost constant. Their distributions have similar profiles whereas, in the ribbed bend pipe, both streamwise and tangential turbulence intensities show an increase in the region corresponds to $0.4 < r/R \leq 0.7$ then gradually decrease near the wall where $r/R > 0.7$. It follows that the highest turbulence intensities in the absence of the ribs are relatively low compared to those in the case with ribs where the turbulence intensities in both streamwise and transverse directions peaks downstream of the ribs then gradually decrease away from the ribs; however, the extent of the maximum values is much higher in both directions.

Re-examining Fig. 8 to 10 again, it appears that the turbulence intensities for both cases considered does not change too much for a wide range of Dean number. This does not mean that the flow becomes less turbulent but we simply say that the velocity fluctuations divided by the mean velocity decreases.

From the above, it is concluded that the turbulence intensities are significantly increased in the ribbed pipe and the flow seems highly turbulent owing to the presence of the ribs.

6.3 Reynolds Shear Stresses

Figure 11, 12 and 13 illustrate respectively the evolution of three components of Reynolds stress $\overline{u'v'}$, $\overline{u'w'}$ and $\overline{v'w'}$ that represent the loss of mechanical energy by the main flow due to its interaction with turbulence. The determination of these turbulent stresses provides an understanding of the shear dispersion in the flow which is the central problem of turbulence.

The examination of Fig. 11 shows that in the case of the bend pipe without ribs, the Reynolds stress component $\overline{u'v'}$ has a small positive value in the region $r/R \geq 0.8$ accompanied with a smaller magnitude and it is negligible for $r/R < 0.8$. Whereas, in the case of the bend pipe with ribs, it is observed that the stress is nearly positive through the range in which the measurements are performed and it maximizes downstream of the ribs where its peak value extends to a higher non-dimensional height near the wall then decreases in magnitude to approximately 70% of its former level corresponding to the value near the wall. This maximization results in an increased production leading to an improvement in the turbulent kinetic energy in the heart of the bend pipe. It is also noticed, that the peak position is almost the same for all measurements.

For both cases considered with and without ribs, as can be seen, near the axial centerline, the fluctuations are less important than those near the wall. Consequently, the magnitudes of the shear stresses are significantly reduced and should be identically zero as shown in Fig. 11 which indicating that in this region, the turbulence is fairly uniform (isotropic turbulence).

For the component $\overline{u'w'}$, we observe clearly the same behavior as that of the component $\overline{u'v'}$ making the production of stresses in those two directions equal, (see Fig. 12).

From the above, it is clear by comparison that, the convection and diffusion of the $\overline{u'v'}$, $\overline{u'w'}$ stresses in the case of the bend without ribs, are extremely small than the case of ribbed bend pipe. It clearly means that the stress components are elevated in the presence of ribs.

Considering the comparisons of the evolution of turbulent shear stress $\overline{v'w'}$ shown in Fig. 13, the profiles show a change in sign of the stress indicating two peaks value. This demonstrates that, the Reynolds stress changes behavior near the separation point where it varies sign accompanied with a smaller magnitude compared to the $\overline{u'v'}$ and $\overline{u'w'}$ stresses. This change in sign is certainly linked to the secondary flow motion which disturbs the velocity field to the point where the sign of the gradient is modified.

By comparison of the two cases considered (with and without ribs), we observe that the peak value of the Reynolds shear stresses is almost the same while the peak position is different. It appears also that the behavior of Reynolds stresses is strongly related to the Dean number. This results in the fact that as the Dean number increases, the effect on the velocity fluctuations becomes weaker. This shows that turbulence fluctuations are reduced much less by the flow control at higher Dean numbers.

7. Conclusions

In the present study, a numerical simulation of the three dimensional unsteady and anisotropic turbulent flow of single-phase incompressible fluid through two 90° bend pipes one without ribs and the other with ribs were carried in ANSYS Fluent solver using realizable RSM turbulence model. A large Dean number range from 5000 to 40000 was tested for each geometry in order to investigate its effect on flow characteristics. For both bend pipe cases considered (with and without ribs), the process of formation of different profiles representing the dynamic and turbulent characteristics of the analyzed flow, in the straight section, downstream the bend, was taken into consideration. A comparison of numerical simulation results between the two considered geometries has been presented in order, to see on the one hand how the analyzed flow behaves dynamically in 90° bend pipes and on the other hand globally evaluate the impact of ribs on the velocity, turbulence intensities and Reynolds shear stresses. The conclusions based on the analysis of obtained results are presented as follows:

- The feasibility of closures, which in principle ensures that the solutions obtained with the RSM model have a physical meaning by not allowing the production of negative normal stresses of the Reynolds tensor, is obtained. Moreover, it was also observed that the Reynolds stress model (RSM) successfully predicts the peak shear stresses.
- Near the bend, it was observed for both cases with and without ribs that the maximum value of the U_x/u_{in} is located near the outer wall. However as it moved away from the curvature it was found that the maximum is located more towards the centerline in the bend pipe with ribs than that in the case without ribs. It can be clearly noted that the profile of U_x/u_{in} in the ribbed case does not resemble the profile of the non-ribbed case, emphasizing the fact that the core flow is affected by the presence of the ribs. As a result, the higher resistance generated by the ribs produced relatively larger velocity gradient ($\partial U/\partial y$) compared to the case of bend pipe without ribs where a more uniform mean velocity profile is observed.
- It is observed, that the measurements of the turbulence intensities of analyzed flow at different positions downstream the bend, is very low dependence on Dean number whether with or without ribs. It seems that the turbulence intensities are higher in the ribbed bend pipe (up to 15% at $r/R=0$) compared to those in the non-ribbed case (between 5% and 10% at $r/R=0$). This means that because of the ribs, the interaction process increases significantly the values of intensities. It was also found that in the ribbed bend pipe, the maximum turbulence intensities showed high values near the wall.
- For the Reynolds shear stresses examined, our results show that the Dean number has notable effects on the peak value of the component $\overline{v'w'}$ compared to the two other components $\overline{u'w'}$ and $\overline{u'v'}$. The analysis of these stresses distribution showed that the ribs enhanced the levels of the Reynolds shear stresses significantly compared to the case without ribs. This increasing is explained by significantly higher levels of turbulence production over those ribs (produced by large values of $\partial U/\partial y$).
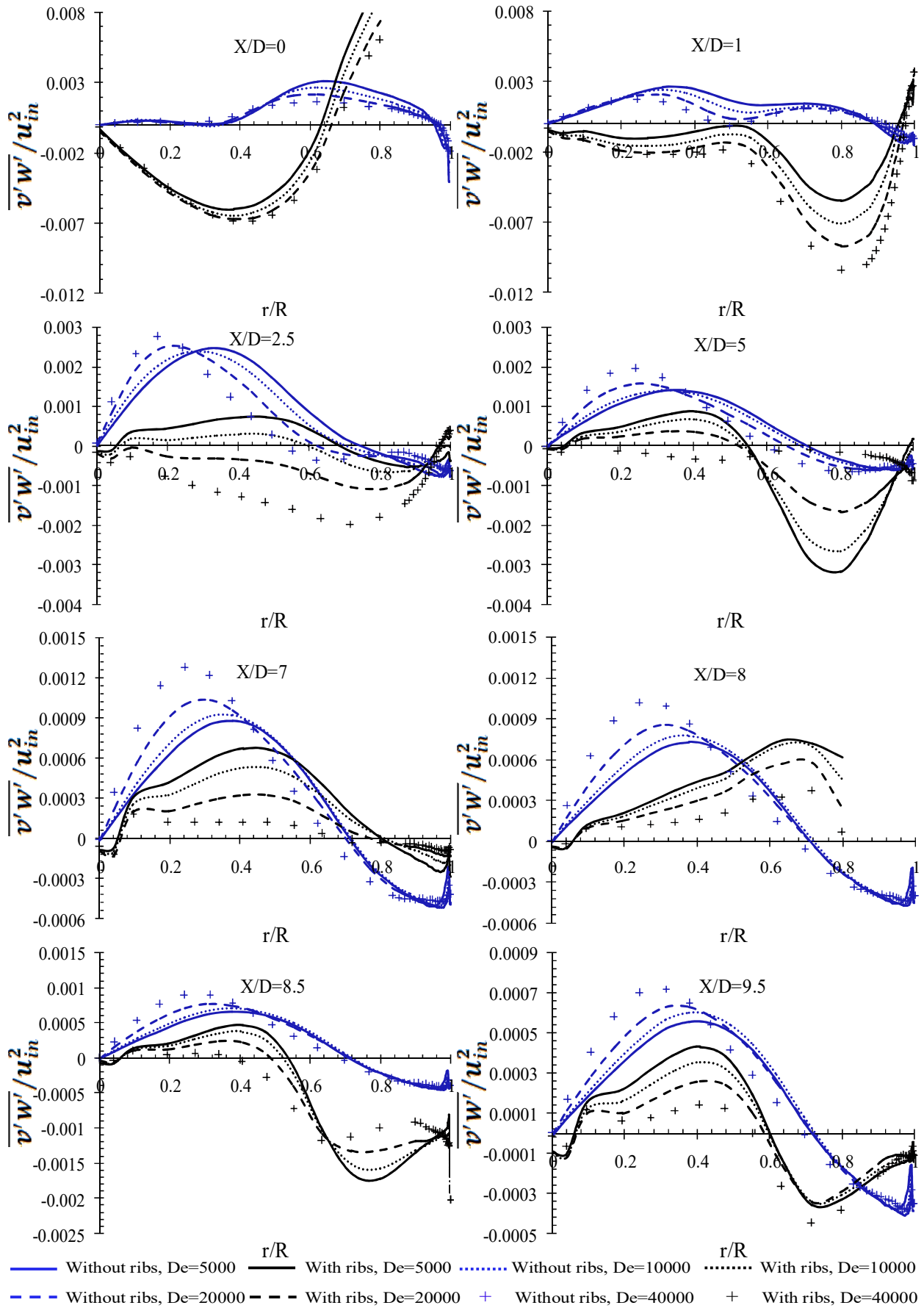
Fig. 13. Comparison of the normalized Reynolds shear stress $\overline{v'w'}/u_{in}^2$ distributions between the ribbed and non-ribbed bend pipe at selected locations downstream the bend, De=5000, 10000, 20000 and 40000.

Author Contributions

In this paper, the main idea, the numerical simulations and the mathematical calculations are conducted by R. Chiremsel and A. Fourar; F. Massouh participated in the analyses of the results of simulations in consultation with R. Chiremsel and A. Fourar; Z. Chiremsel wrote the manuscript. The manuscript was written through the contribution of all authors. All authors discussed the results, reviewed and approved the final version of the manuscript.

Conflict of Interest

The authors declared no potential conflicts of interest with respect to the research, authorship, and publication of this article.

Funding

Nomenclature

Cp	Specific heat [J.kg^{-1}.K^{-1}]	u_i	Velocity vector [m/s]
d	Normal distance to the wall [m]	u'_i	Fluctuating velocity vector [m/s]
D	Pipe diameter [m]	u_{in}	Inlet velocity [m/s]
De	Dean number	U_x	Axial mean velocity [m/s]
e	Rib height [m]	x_i	Coordinate vector [m]
I	Turbulence intensity	y+	Non–dimensional distance from the wall
k	Turbulent kinetic energy [m^2/s^2]	δ_{ij}	Kronecker symbol
K	Thermal conductivity [W.m^{-1}.k^{-1}]	ε	Turbulence dissipation rate [m^2/s^3]
p_i	Instantaneous pressure [Pa]	ε_{in}	Turbulence dissipation rate tensor [m^2/s^3]
p'_i	Fluctuating pressure [Pa]	κ	Von Kármán constant
Pt	Rib pitch [m]	μ	Dynamic viscosity [kg/m.s]
R	Radius of pipe [m]	μ_t	Dynamic turbulent viscosity [kg/m.s]
Rc	Curvature radius of pipe [m]	υ	Kinematic viscosity [m^2/s]
Re	Reynolds number	ρ	Density [kg/m^3]
t	Time [s]		

References

[1] Vasiliy, S., Pavel, K., Vitaliy, S., Fedor, P., Method of Unsteady Hydrodynamic Characteristics Determination in Turbulent Boundary Layer, *Journal of Applied and Computational Mechanics*, 7(2), 2021, 849-857.

[2] Lumley, J.L., Computational Modeling of Turbulent Flows, *Advances in Applied Mechanics*, 18, 1979, 161-178.

[3] Sheikholeslami, M., Farshad, S.A., Nanoparticle Transportation inside a Tube with Quad-Channel Tapes involving Solar Radiation, *Powder Technology*, 378, 2021, 145-159.

[4] Sudo, K., Sumida, M., Hibara, H., Experimental Investigation on Turbulent Flow in a Circular-Sectioned 90-Degree Bend, *Experiments in Fluids*, 25, 1998, 42-49.

[5] Hüttl, T.J., Friedrich, R., Direct Numerical Simulation of Turbulent Flows in Curved and Helically Coiled Pipes, *Computers & Fluids*, 30, 2001, 591-605.

[6] Kawamura, T., Nakao, T., Takahashi, M., Reynolds Number Effect on Turbulence Downstream from Elbow Pipe, *Trans, Transactions of the Japan Society of Mechanical Engineers Series B*, 68(667), 2002, 645-651.

[7] Chang, T.H., Lee, H.S., An Experimental Study on Swirling Flow in a 90 Degree Circular Tube by using Particle Image Velocimetry, *Journal of Visualization*, 6, 2003, 343-352.

[8] Spedding, P.L., Benard, E., McNally, G.M., Fluid Flow through 90˚ Bends, *Developments in Chemical Engineering and Mineral Processing*, 12(1-2), 2008, 107-128.

[9] Pruvost, J., Legrand, J., Legentilhomme, P., Numerical Investigation of Bend and Torus Flows, Part I: Effect of Swirl Motion on Flow Structure in U-bend, *Chemical Engineering Science*, 59(16), 2004, 3345-3357.

[10] Raisee, M., Alemi, H., Iacovides, H., Prediction of Developing Turbulent Flow in 90°-Curved Ducts using Linear and Non-Linear Low-Re k-ε Models, *International Journal for Numerical Methods in Fluids*, 51(12), 2006, 1379-1405.

[11] Crawford, N.M., Cunningham, G., Spence, S.W.T., An Experimental Investigation into the Pressure Drop for Turbulent Flow in 90° Elbow Bends, *Proceedings of the Institution of Mechanical Engineers, Part E: Journal of Process Mechanical Engineering*, 221(2), 2007, 77-88.

[12] Shiraishi, T., Watakabe, H., Sago, H., Konomura, M., Ymaguchi, A., Fujii, T., Resistance and Fluctuating Pressure of a Large Elbow in High Reynolds Numbers, *Journal of Fluid Mechanics*, 128(5), 2006, 1063-1073.

[13] Shiraishi, T., Watakabe, H., Sago, H., Yamano, H., Pressure Fluctuation Characteristics of the Short Radius Elbow Pipe for FBR in the Postcritical Reynolds Regime, *Journal of Fluid Science and Technology*, 4(2), 2009, 430-441.

[14] Mojtaba, J., Cathy, C., Hassan, P., Secondary Flow Velocity Field in Laminar Pulsating Flow through Curved Pipes-Piv Measurements, *Proceedings of the ASME 2009 Fluids Engineering Division Summer Meeting*, 78141, 2009, 1577-1584.

[15] Ono, A., Kimura, N., Kamide, H., Tobita, A., Influence of Elbow Curvature on Flow Structure at Elbow Outlet under High Reynolds Number Condition, *Nuclear Engineering and Design*, 241(11), 2011, 4409-4419.

[16] Noorani, A., El Khoury, G.K., Schlatter, P., Evolution of Turbulence Characteristics from Straight to Curved Pipes, *International Journal of Heat and Fluid Flow*, 41, 2013, 16-26.

[17] Min, C., Zhiguo, Z., Numerical Simulation of Turbulent Driven Secondary Flow in a 90° Bend Pipe, *Advanced Materials Research*, 765-767, 2013, 514-519.

[18] Niu, L., Dou, H-S., Stability Study of Flow in a 90° Bend Based on the Energy Gradient Theory, *6th International Conference on Pumps and Fans with Compressors and Wind Turbines, IOP Conf. Series: Materials Science and Engineering*, 52(2013), 2013, 022006.

[19] Hellström, L.H.O., Zlatinov, M.B., Cao, G., Smits, A.J., Turbulent Pipe Flow Downstream of a 90° Bend, *Journal of Fluid Mechanics*, 735, 2013, R7.

[20] Jongtae, K., Mohan, Y., Seungjin, K., Characteristics of Secondary Flow Induced by 90-Degree Elbow in Turbulent Pipe Flow, *Engineering Applications of Computational Fluid Mechanics*, 8(2), 2014, 229-239.

[21] Dutta, P., Nandi, N., Effect of Reynolds Number and Curvature Ratio on Single Phase Turbulent Flow in Pipe Bends, *Mechanics and Mechanical Engineering*, 19(1), 2015, 5-16.

[22] Yan, W., Quanlin, D., Pengfei, W., Numerical Investigation on Fluid Flow in a 90-Degree Curved Pipe with Large Curvature Ratio, *Mathematical*

Problems in Engineering, 15, 2015, 548262.

[23] Röhrig, R., Jakirlic´, S., Tropea, C., Comparative Computational Study of Turbulent Flow in a 90° Pipe Elbow, *International Journal of Heat and Fluid Flow*, 55, 2015, 120-131.

[24] Wang, Z., Örlü, R., Schlatter, P., Chung, Y.M., Direct Numerical Simulation of a Turbulent Curved Pipe Flow, *International Journal of Heat and Fluid Flow*, 73, 2018, 199-208.

[25] Dutta, P., Saha, S.K., Nandi, N., Pal, N., Numerical Study on Flow Separation in 90° Pipe Bend under High Reynolds Number by k-ε Modelling, *Engineering Science and Technology, an International Journal*, 19, 2016, 904-910.

[26] Belhoucine, L., Deville, M., Elazehari, A.R., Bensalah, M.O., Explicit Algebraic Reynolds Stress Model of Incompressible Turbulent Flow in Rotating Square Duct, *Computers & Fluids*, 33(2), 2004, 179-199.

[27] Sowjanya, V., Jie, C., Performance of Turbulence Models for Flows Through Rough Pipes, *Applied Mathematical Modelling*, 34, 2010, 1458-1466.

[28] Adam, A., Zhiyin, Y., Yiling, L., Computational Analysis of Turbulent Flow over a Bluff Body with Drag Reduction Devices, *Journal of Applied and Computational Mechanics*, 6(SI), 2020, 1210-1219.

[29] Balen, W.V., Uijttewaal, W. S. J., Blanckaert, K., Large-Eddy Simulation of a Mildly Curved Open-Channel Flow, *Journal of Fluid Mechanics*, 630, 2009, 413-442.

[30] Ha, M.H., Numerical Prediction of Turbulent Flows in Engineering, *SHF*, 1987, 555-562.

[31] Honoré, G., *Numerical Analysis of Anisotropic Turbulent Flows using Nonlinear Turbulence Models*, Ph. D. Thesis, Polytechnic of Lille, 2008.

[32] Launder, B.E., Second-Moment Closure: Present … and Future?, *International Journal of Heat and Fluid Flow*, 10(4), 1989, 282-300.

[33] Lai, Y.G., So, R.M.C., Anwer, M., Hwang, B.C., Calculations of a Curved Pipe Flow using Reynolds Stress Closure, *Proceedings of the Institution of Mechanical Engineers, Part C: Journal of Mechanical Engineering Science*, 205, 1991, 231-244.

[34] Richard, W.J., Modeling Strategies for Unsteady Turbulent Flows in the Lower Plenum of the VHTR, *Nuclear Engineering and Design*, 238(3), 2008, 482-491.

[35] Carsten, S., Manfred, Z., The Influence of Loading Position in a Priori High Stress Detection using Mode Superposition, *Reports in Mechanical Engineering*, 1(1), 2020, 93-102.

[36] Kumar, V., Frohnapfel, B., Jovanović, J., Breuer, M., Zuo, W., Hadzić, I., Lechner, R., Anisotropy Invariant Reynolds Stress Model of Turbulence (AIRSM) and its Application to Attached and Separated Wall-Bounded Flows, *Flow Turbulence Combust.*, 83, 2009, 81-103.

[37] Al-Sharif, S.F., Cotton, M.A., Craft, T.J., Reynolds Stress Transport Models in Unsteady and Non-Equilibrium Turbulent Flows, *International Journal of Heat and Fluid Flow*, 31, 2010, 401-408.

[38] Lien, F.S., Leschziner, M.A., Assessment of Turbulent Transport Models including Non-Linear Rbg Eddy-Viscosity Formulation and Second-Moment Closure, *Computers and Fluids*, 23(8), 1994, 983-1004.

[39] Gibson, M.M., Launder, B.E., Ground Effects on Pressure Fluctuations in the Atmospheric Boundary Layer, *Journal of Fluid Mechanics*, 86, 1978, 491-511.

[40] Fu, S., Launder, B.E., Leschziner, M.A., Modeling Strongly Swirling Recirculating Jet Flow with Reynolds-Stress Transport Closures, *Sixth Int. Symposium on Turbulent Shear Flows*, 7-9 September, Toulouse, France, 1987.

[41] ANSYS Fluent Theory Guide, Release 19.0, January, 2018.

[42] Sarkar, S., Balakrishnan, L., Application of a Reynolds Stress Turbulence Model to the Compressible Shear Layer, *AIAA Journal*, 29(5), 1991, 743-752.

[43] Chien, L.H., Liao, W.R., Ghalambaz, M., Yan, W.M., Experimental Study on Convective Boiling of Micro-Pin-Finned Channels with Parallel Arrangement Fins for FC-72 Dielectric Fluid, *International Journal of Heat and Mass Transfer*, 138, 2019, 390-400.

[44] Nematollahi, M.R., Nazifi, M., Enhancement of Heat Transfer in a Typical Pressurized Water Reactor by Different Mixing Vanes on Spacer Grids, *Energy Conversion and Management*, 49(7), 2008, 1981-1988.

[45] Živan, S., Miloš, J., Jasmina, B.J., Saša, M., Numerical Investigation of the Influence of the Doubly Curved Blade Profiles on the Reversible Axial Fan Characteristics, *Facta Universitatis-Series Mechanical Engineering*, 18(1), 2020, 57-68.

[46] Versteeg, H.K., Malalasekera, W., *An Introduction to Computational Fluid Dynamics-The Finite Volume Method*, Pearson Education Limited, Harlow, Second Edition, ISBN 978-0-13-127498-3, 2007.

[47] Miroslav, M., Sonja, V., Dušan, Ć., Dragan, M., Numerical Simulation of Fluid-Structure Interaction Between Fishing Wobbler and Water, *Facta Universitatis-Series Mechanical Engineering*, 18(4), 2020, 665-676.

[48] Quamrul, H.M., CFD Analysis of Single and Multiphase Flow Characteristics in Elbow, *Scientific Research*, 4(4), 2012, 210-214.

[49] ANSYS Meshing User's Guide, ANSYS Inc, Southpointe 2600 ANSYS Drive Canonsburg, PA 15317, 2018.

[50] Pavel, P., Dejan, B., Suitability for Coding of the Colebrook's Flow Friction Relation Expressed by Symbolic Regression Approximations of the Wright-ω Function, *Reports in Mechanical Engineering*, 1(1), 2020, 174-179.

[51] Ho, C.J., Liu, Y.C., Ghalambaz, M., Yan, W.M., Forced Convection Heat Transfer of Nano-Encapsulated Phase Change Material (NEPCM) Suspension in a Mini-Channel Heatsink, *International Journal of Heat and Mass Transfer*, 155, 2020, 1-13.

[52] Ho, C.J., Liu, Y.C., Yang, T.F., Ghalambaz, M., Yan, W.M., Convective Heat Transfer of Nano-Encapsulated Phase Change Material Suspension in a Divergent Minichannel Heatsink, *International Journal of Heat and Mass Transfer*, 165, 2021, 1-40.

[53] Chien, L.H., Cheng, Y.T., Lai, Y.L., Yan, W.M., Ghalambaz, M., Experimental and Numerical Study on Convective Boiling in a Staggered Array of Micro Pin-Fin Microgap, *International Journal of Heat and Mass Transfer*, 149, 2020, 1-16.

[54] Sheikholeslamia, M., Farshad, S.A., Shafee, A., Babazadeh, H., Performance of Solar Collector with Turbulator involving Nanomaterial Turbulent Regime, *Renewable Energy*, 163, 2021, 1222-1237.

ORCID iD

Rachid Chiremsel https://orcid.org/0000-0002-3048-7206
Ali Fourar https://orcid.org/0000-0003-2612-3589
Fawaz Massouh https://orcid.org/0000-0002-0718-5429
Zakarya Chiremsel https://orcid.org/0000-0002-7236-137x

Publisher's Note Shahid Chamran University of Ahvaz remains neutral with regard to jurisdictional claims in published maps and institutional affiliations.